(Received 14 November 2025, Accepted 10 December 2025, Scheduled 4 March 2026)

A Frequency and Linear Polarization Reconfigurable Printed Dipole Antenna

Yulian Ruan, Shixing Yu*, and Na Kou

College of Big Data and Information Engineering, Guizhou University, Guiyang 550025, China

ABSTRACT: In this letter, a frequency and linear-polarization (LP) reconfigurable antenna is proposed. The antenna consists of two pairs of printed dipoles as the primary radiating patches. By independently controlling the direction of the flowing current using loaded PIN diodes, the dynamic reconfiguration of both frequency and linear polarization can be realized. In addition, a dual-band artificial magnetic conductor (AMC) reflector is added under the radiator, which can effectively reduce the antenna profile to $0.1\lambda_0$ (12.4 mm, where λ_0 is the wavelength at low operating frequency). Both simulated and experimental results show that the proposed antenna can operate in four modes: 0° LP low-frequency (2.36–2.77 GHz) state, 0° LP high-frequency (3.25–3.68 GHz) state, 90° LP low-frequency state, and 90° LP high-frequency state. The antenna exhibits stable radiation patterns, with gain values of 7.56 dBi in the low-frequency state and 8.03 dBi in the high-frequency state. This antenna is suitable for ISM band applications, such as Wi-Fi (2.4–2.48 GHz) and Bluetooth (2.4–2.48 GHz), as well as TDD Band 42, meeting the requirements of modern wireless communication systems.

1. INTRODUCTION

The development of wireless communication technology has led to an increasingly complex electromagnetic environment, in which traditional fixed antennas can hardly meet the diverse and dynamically changing communication requirements. It has led to an increased demand for reconfigurable antennas, which can adapt to these changing requirements. There are several types of reconfigurable antennas, including radiation direction [1], frequency [2, 3], and polarization [4, 5] reconfigurations. Reconfigurable features are generally achieved by introducing electronically controlled switches into the antenna structure, such as PIN diodes [6], microelectromechanical system (MEMS) [7], and varactors [8]. They are capable of adjusting the operation mode of the antenna, thus realizing performance reconfiguration. For example, a frequency reconfigurable slot-loop antenna was proposed in [9], whose operating frequency can be switched from L-band to C-band. In general, frequency reconfigurability is usually achieved by changing the effective electrical length of the antenna in order to realize the electrical tunability of the operating band [10, 11].

Furthermore, adjusting the linear polarization (LP) state of antenna can reduce signal fading and improve the quality and efficiency of signal transmission [12]. A multi-linear polarization (multi-LP) reconfigurable patch antenna is proposed in [13], which can switch among four LPs per 45° rotation by introducing a combination of mechanical rotation and electrical adjustment. In order to flexibly control the LP reconfiguration, it has been investigated to use coaxial cables to feed the printed dipoles and obtain LP reconfigurability by controlling the current flow across the printed dipoles [14, 15]. However, single frequency or polarization reconfigurable antenna cannot meet the modern antenna requirements especially when the wireless communication systems need to provide multi-functions or services.

Hence, frequency- and polarization-reconfigurable antennas have been extensively investigated to reduce the number of antenna elements and the occupied volume in modern wireless systems [16–21]. Various techniques have been proposed to achieve both frequency and linear-polarization reconfigurability within a single antenna aperture. One common approach is to introduce multiple resonant paths or cavity modes loaded with PIN diodes or varactors, so that both the effective electrical length and the current distribution of the radiator can be modified, enabling the control of operating bands and polarization states [16, 17]. Another approach is to employ metasurface- or AMC-based hybrid structures, in which tunable or switchable units are utilized to manipulate the resonant frequencies and generate orthogonal linear or circular polarizations [18, 19]. Moreover, miniaturized capacitance-loaded antennas have been used to realize compact circularly polarized reconfigurable designs, where the loading capacitances provide additional degrees of freedom to control the resonance and polarization states [20]. Furthermore, liquid and flexible antennas exploit shape reconfiguration and tunable feeding networks to achieve multi-state linear and circular polarizations (e.g., LP/LHCP/RHCP) together with wideband frequency tuning [21].

However, many frequency- and polarization-reconfigurable antennas have been implemented using printed dipole structures, and the spacing between the dipole and the ground plane is typically around a quarter wavelength, leading to a high profile. Using an AMC reflector can effectively reduce the height of a printed dipole antenna, and it has been widely used [22–25]. An AMC structure with cross-shaped patches has been

* Corresponding author: Shixing Yu (sxyu1@gzu.edu.cn).

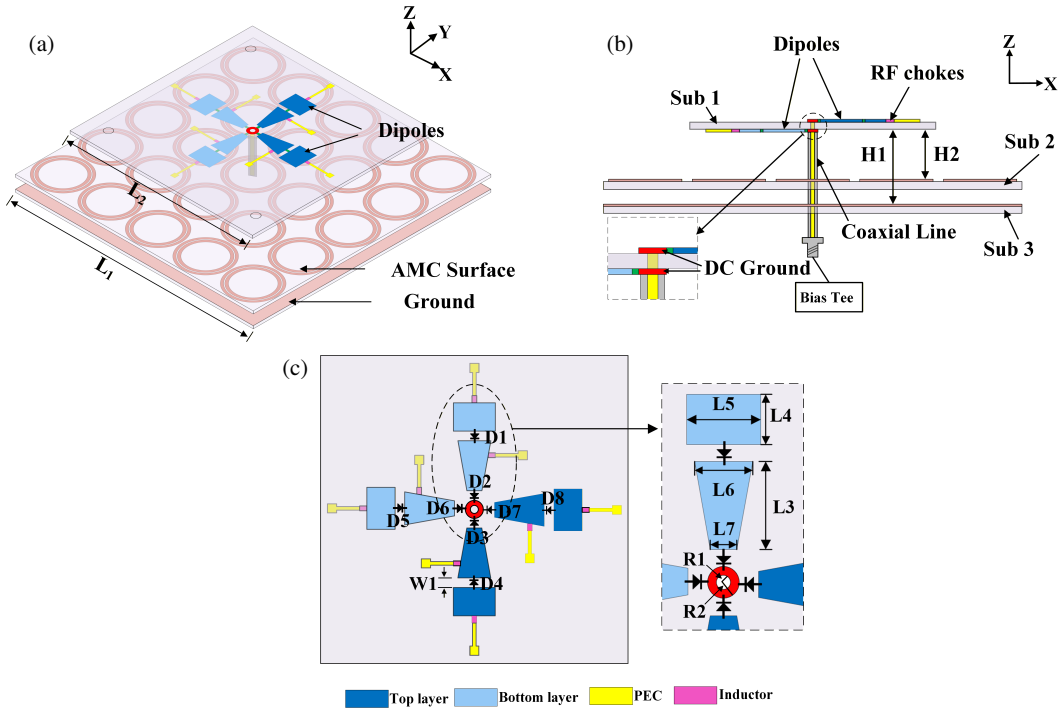

FIGURE 1. Configuration of the proposed antenna. (a) Perspective view, (b) side view, (c) top view of dipole. The parameters of the structure are: $L1 = 112.5\,\text{mm}$, $L2 = 76\,\text{mm}$, $L3 = 9.5\,\text{mm}$, $L4 = 5.9\,\text{mm}$, $L5 = 7\,\text{mm}$, $L6 = 5.5\,\text{mm}$, $L7 = 2\,\text{mm}$, $H1 = 12.4\,\text{mm}$, $H2 = 8.8\,\text{mm}$, $R1 = 0.8\,\text{mm}$, $R2 = 1.5\,\text{mm}$, $W1 = 0.42\,\text{mm}$.

proposed in [26], which can provide a wide bandwidth and reduce the antenna profile. In addition, the dual-band AMC structures have also been studied [27, 28].

In this letter, a frequency and LP reconfigurable printed dipole antenna is proposed. By embedding PIN diodes into segmented dipole arms and properly controlling the current paths, the antenna provides four distinct operating modes, i.e., two switchable operating bands combined with two orthogonal linear polarization (LP) states (0° and 90°). A dual-band AMC reflector is designed to offer in-phase reflection in both bands, enabling a low profile of $0.1\lambda_0$ while preserving wide impedance bandwidth and stable broadside radiation patterns. Compared with previously reported frequency- and polarization-reconfigurable antennas, the main contributions of this work can be summarized as follows: (1) a compact printed dipole element that simultaneously realizes dual-band and dual-LP reconfigurability through a simple PIN-diode biasing network, and (2) a passive dual-band AMC-backed configuration that achieves significant profile reduction without noticeable degradation of radiation performance, with measured gains of 7.56 dBi and 8.03 dBi in the lower and upper bands, respectively, making the antenna attractive for Industrial, Scientific, and Medical (ISM)-band (2.4–2.48 GHz Wi-Fi/Bluetooth) and TDD Band 42 applications.

2. ANTENNA DESIGN

2.1. Antenna Structures

The structure of the proposed antenna is shown in Fig. 1(a), which consists of three layers of FR4 dielectric sheets with a thickness of 1 mm. The relative dielectric constant is 4.4, and the loss angle tangent is 0.02. Two pairs of segmented printing dipole patches are used for radiation, each with half part etched on the lower surfaces of the top dielectric sheet and the other part etched on the upper side. The middle dielectric substrate is printed with 5×5 dual-ring periodic cells, forming an AMC-based reflector and thus reducing the overall height of the antenna profile. The bottom dielectric sheet serves as a metal reflector to improve the radiation efficiency of the antenna. The distance from Sub 1 to Sub 2 is 8.8 mm ($0.09\lambda_0$, where λ_0 is the free space wavelength at designed center operating frequency of 2.4 GHz), and that from Sub 1 to Sub 3 is 12.4 mm ($0.1\lambda_0$).

Figures 1(b) and (c) show the feeding structure and DC bias circuit of the antenna. The segmented printing dipole antenna is composed of a trapezoidal patch and a rectangular one connected by a PIN diode. The four trapezoidal patches are connected to the feeding structure at the center by four PIN diodes. Both pairs of printed dipoles are fed by a central coaxial feed line. Specifically, the inner core and outer shell of the coaxial feed line are soldered to the upper and lower circular patches of Sub 1 at the center (marked by red), which also serve as the DC ground for the PIN diodes. A bias tee element is connected to the end of the coaxial feed line to effectively prevent DC current from flowing back to the signal source and to ensure continuous and stable transmission of radio frequency (RF) signals.

At the ends of each trapezoidal and rectangular patch, a narrow DC line with a width of 0.6 mm is routed to connect the other terminal of the PIN diode to the choke inductor. The other end of the inductor is connected to the DC line. For each dipole, two DC lines are connected to small rectangular

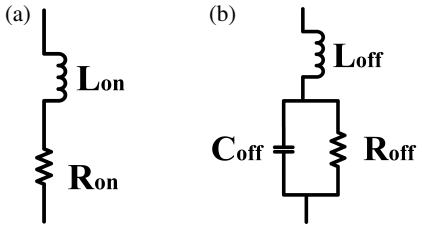

FIGURE 2. Equivalent circuit for the PIN diode in case of (a) ON state and (b) OFF state. ($L_{on} = 0.45\,\text{nH}$, $R_{on} = 0.85\,\Omega$, $L_{off} = 0.45\,\text{nH}$, $R_{off} = 5\,\text{k}\Omega$, $C_{off} = 0.21\,\text{pF}$).

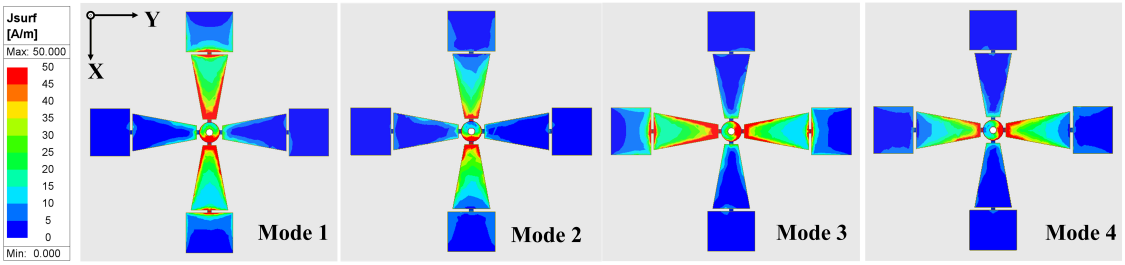

FIGURE 3. The current distribution on the surface of the dipole under four working states.

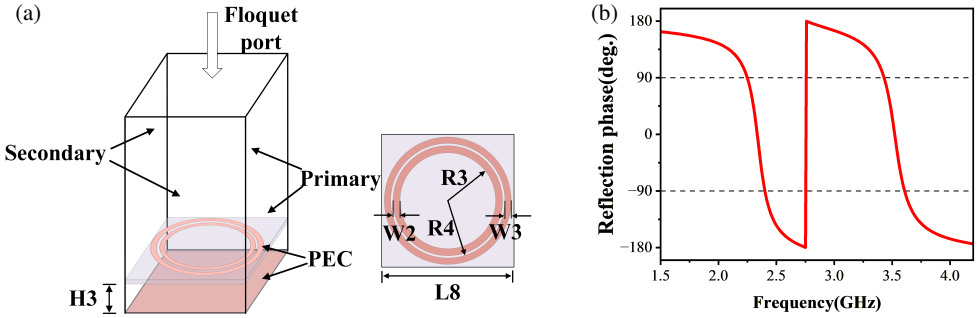

FIGURE 4. (a) AMC unit cell. (b) Simulated reflection phase for AMC unit. (Size parameters: $H3 = 2.6\,\text{mm}$, $L8 = 22.5\,\text{mm}$, $R3 = 8.3\,\text{mm}$, $R4 = 9.9\,\text{mm}$, $W2 = 1.2\,\text{mm}$, $W3 = 1.1\,\text{mm}$).

patches. Each pair of PIN diodes in one branch is forward-biased, and the antenna can operate in the low-frequency state. When the DC line is connected to the trapezoidal patch side, only the PIN diode near the coaxial feed is turned ON, and the antenna operates in the high-frequency state. Table 1 shows different operating modes of the antenna when different combinations of PIN diodes are controlled. The PIN diode with the type of SPM1340-040LF from Skyworks Solutions and the inductor with the type of MLI1608F-R33KT from MetalLionsworks Solutions are used in this design. Fig. 2 shows the equivalent circuit model of the PIN diode in its ON and OFF states. Fig. 3 shows the current distribution on the surface of the dipole under four working states.

TABLE 1. Antenna modes controlled by PIN diodes.

Mode	ON State	OFF State	Linear Pol.	Freq. Range
Mode 1	D1, D2, D3, D4	D5, D6, D7, D8	0° linear pol.	Low
Mode 2	D2, D3	D1, D4, D5, D6, D7, D8	0° linear pol.	High
Mode 3	D5, D6, D7, D8	D1, D2, D3, D4	90° linear pol.	Low
Mode 4	D6, D7	D1, D2, D3, D4, D5, D8	90° linear pol.	High

2.2. AMC Design and Simulation Results

For the printing dipole antenna, the metal ground plane needs to be placed 1/4 wavelength below the antenna to enhance the forward radiation. However, this will inevitably increase the profile height of the antenna, which is bulky for practical applications. In this letter, an AMC structure is placed between the antenna and the metal ground, which can reduce the antenna height. At the resonant frequency, the reflection phase of AMC unit corresponds to 0°, thus realizing the function of a reflector. In general, the effective operating bandwidth can be determined

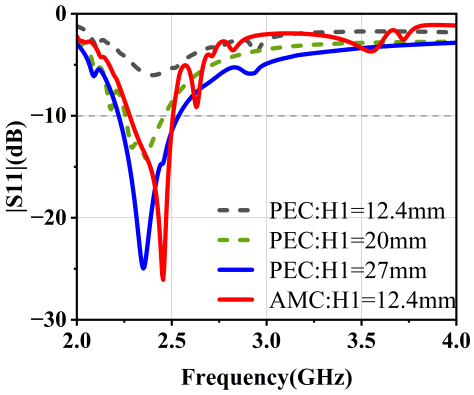

FIGURE 5. Comparison of the reflection coefficients in different cases.

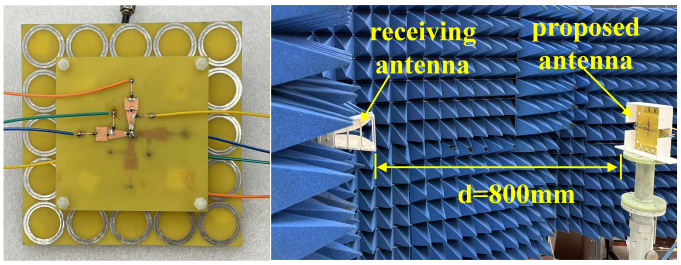

FIGURE 6. Fabricated antenna prototype and measurement in the anechoic chamber.

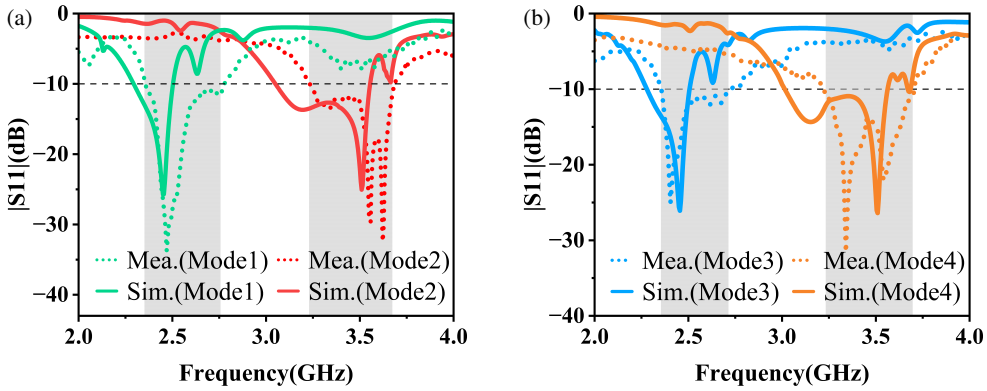

FIGURE 7. Comparison of reflection coefficients between simulation and measurement. (a) Mode 1 and Mode 2; (b) Mode 3 and Mode 4.

by the reflection phase range between $+90°$ and $-90°$ for the AMC unit cell [22].

Since the reconfigurable antenna has two switchable operating frequency range, the AMC unit needs to work at dual bands. Therefore, the AMC unit adopts a dual-ring design, in which the dual-ring patch is printed on an FR-4 dielectric substrate with a thickness of 1 mm. The inner ring adjusts the low-frequency operating point. The AMC unit cell is shown in Fig. 4(a), and its simulated reflection coefficient is shown in Fig. 4(b). We can see that the dual-ring AMC unit cell can operate within two frequency bands: 2.24–2.40 GHz and 3.43–3.60 GHz.

Figure 5 shows the simulated $|S_{11}|$ of one pair of printing dipole antenna with 5×5 AMC and metal ground plane located underneath, respectively. When a metal ground plane (PEC) is used, good impedance matching can only be obtained when the spacing $H1$ is increased to 27 mm ($\approx 0.22\lambda_0$). If $H1$ is reduced to 12.4 mm, the out-of-phase image currents induced by the PEC reflector severely detune the antenna and deteriorate the impedance matching. In contrast, when the proposed dual-band AMC reflector is employed, wideband impedance matching is maintained with a much smaller spacing of $H1 = 12.4$ mm ($0.1\lambda_0$), because the AMC provides an in-phase reflection (with a reflection phase between $-90°$ and $+90°$) over both operating bands. Therefore, the AMC reflector not only reduces the overall profile from about $0.22\lambda_0$ to $0.1\lambda_0$, but also preserves the wide impedance bandwidth of the antenna.

3. ANTENNA PERFORMANCES AND MEASUREMENT

The fabricated antenna prototype is shown in Fig. 6. Fig. 7 shows the simulated and measured reflection coefficients under different operational modes.

It can be seen that when the antenna operates at low frequency (Mode 1 and Mode 3), the simulated bandwidth is 2.28–2.50 GHz while the measured one is 2.36–2.77 GHz. As the antenna operates at high frequency (Mode 2 and Mode 4), the simulated bandwidth is 3.05–3.55 GHz, and the measured one is 3.25–3.68 GHz. The measured operating frequency band shifts to a higher range than the simulation, which is mainly caused by the fact that the dielectric constant of a practical substrate can vary with frequency and the accuracy of the measuring instrument and calibration.

Figure 8 shows the normalized radiation patterns of the measured and simulated co-polarization (co-pol) and cross-polarization (x-pol) components in the E-plane and H-plane under four modes (mode 1 and mode 3 at 2.4 GHz, mode 2 and mode 4 at 3.4 GHz). It can be seen that under different polarization states, the main beam direction and beamwidth are almost unchanged, and the cross-polarization level is suppressed well, indicating that the linear polarization purity is relatively high. Since the PIN diodes and RF chokes are implemented as electrically small lumped elements and are located along the bias lines, their influence on the current distribution over the radiat-

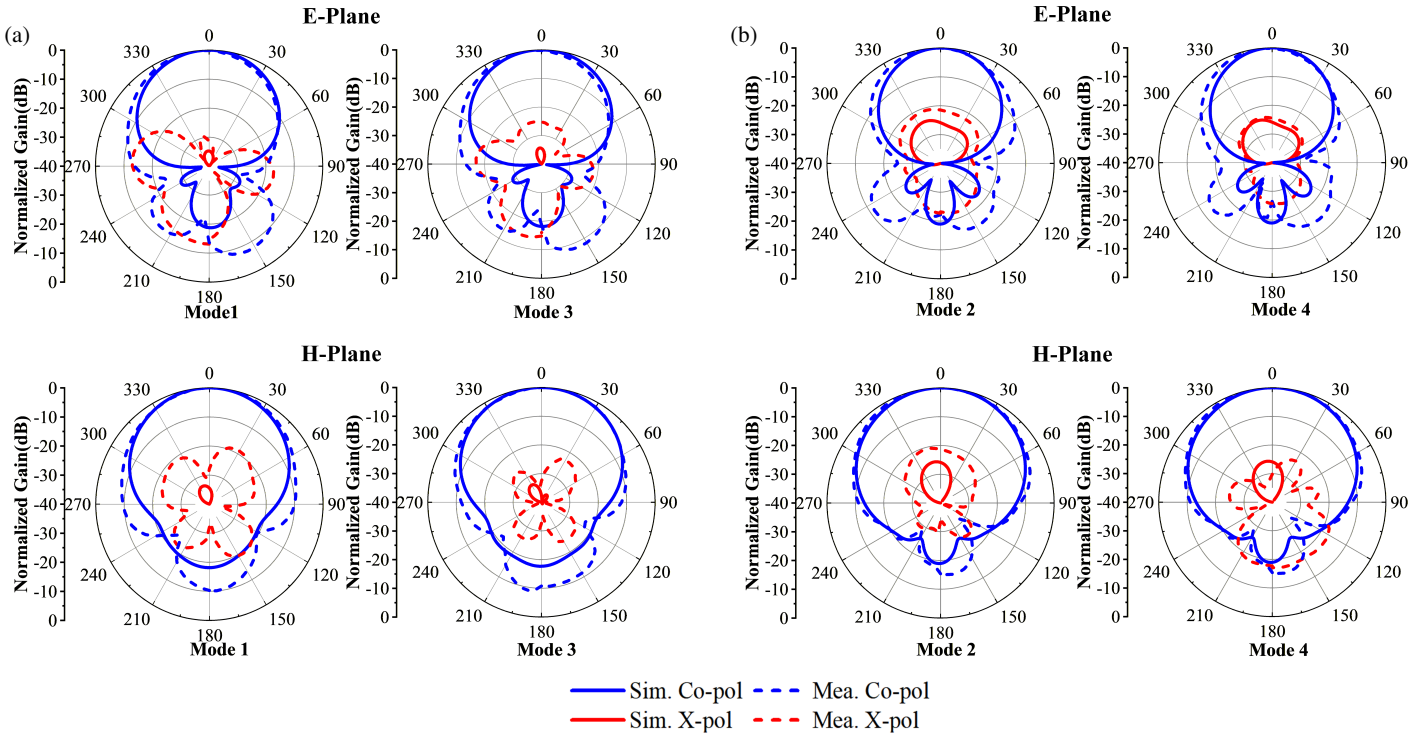

FIGURE 8. Simulated and measured radiation patterns at (a) 2.4 GHz and (b) 3.4 GHz.

TABLE 2. Performances comparison.

Ref	Height (λ_0)	Freq. (GHz)	Gain (dBi)	Reconfigurable
[2]	0.1	3.3–3.6 & 4.8–5.0	6.86 & 8.14	Freq
[12]	0.07	2.33–2.50	5.9	Polar
[13]	0.24	2.2–3.1	5.2	Polar
[18]	0.15	0.2–0.3	5.0	Freq. & Polar
[19]	0.14	2.2–3.5	9.4–9.8	Freq. & Polar
[20]	0.03	0.87–0.96	4.8	Freq. & Polar
[21]	0.17	2.1–2.65	5.4	Freq. & Polar
Prop.	0.1	2.36–2.77 & 3.25–3.68	7.56 & 8.03	Freq. & Polar.

ing dipoles is limited. As a result, the introduction of the PIN diodes and RF chokes does not noticeably distort the radiation patterns in any of the four operating modes.

In Fig. 9, the simulated and measured gains are shown for both frequency bands. The symmetrical configuration of the antenna means that the 0° and 90° polarization modes exhibit the same performance. The measured results show that the antenna has the maximum gains of 7.56 dBi and 8.03 dBi at low and high operating frequencies of 2.4 GHz and 3.4 GHz, respectively. The slight discrepancy between the simulated and measured gains is mainly caused by the additional loss of the PIN diodes, RF chokes, and feed cables, while the overall impact on radiation efficiency remains small.

Finally, Table 2 compares the proposed antenna with some related works. It can be seen that the antenna presented in this letter achieves frequency-reconfigurable operation be-

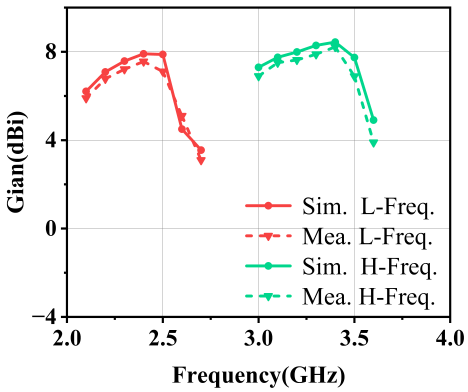

FIGURE 9. Simulated and measured gains of the proposed antenna.

tween two bands and two reconfigurable linear-polarization states (0° and 90°) within a low-profile structure. In particular, it maintains a profile of only $0.1\lambda_0$ while still providing relatively high gains of 7.56 dBi and 8.03 dBi in the two operating bands, which makes it competitive for 2.4 GHz ISM-band applications, such as Wi-Fi and Bluetooth (2.4–2.48 GHz), as well as for TDD Band 42 communications.

4. CONCLUSION

In this letter, a frequency and linear polarization reconfigurable antenna is proposed. The antenna consists of two pairs of vertically aligned segmented printed dipoles coupled with a 5×5 dual-band AMC reflector to reduce the antenna height to $0.1\lambda_0$. By controlling the states of loaded PIN diodes in the printed dipole structures, two frequency bands and two linear polarization states can be switched. Simulation and measurement results show that the antenna can operate in four modes. Under all four modes, the directional pattern of the antenna is stable, and the gain can reach 7.56 dBi at the low band and 8.03 dBi at the high band, meeting the requirements of modern wireless communication systems.

ACKNOWLEDGEMENT

This work was supported in part by the National Natural Science Foundation of China under Grant (62261007, 62361008) and in part by the Guizhou Provincial Basic Research Program (Natural Science) under Grant QKHJC MS [2025] 591.

REFERENCES

[1] Li, J.-F., B. Wu, J.-Q. Zhou, K.-X. Guo, H.-R. Zu, and T. Su, "Frequency and pattern reconfigurable antenna using double layer petal shaped parasitic structure," *IEEE Transactions on Circuits and Systems II: Express Briefs*, Vol. 71, No. 4, 1934–1938, Apr. 2024.

[2] Nie, Z., H. Zhai, L. Liu, J. Li, D. Hu, and J. Shi, "A dual-polarized frequency-reconfigurable low-profile antenna with harmonic suppression for 5G application," *IEEE Antennas and Wireless Propagation Letters*, Vol. 18, No. 6, 1228–1232, Jun. 2019.

[3] Jin, G., C. Deng, Y. Xu, J. Yang, and S. Liao, "Differential frequency-reconfigurable antenna based on dipoles for sub-6 GHz 5G and WLAN applications," *IEEE Antennas and Wireless Propagation Letters*, Vol. 19, No. 3, 472–476, 2020.

[4] Tran, H. H., C. D. Bui, N. Nguyen-Trong, and T. K. Nguyen, "A wideband non-uniform metasurface-based circularly polarized reconfigurable antenna," *IEEE Access*, Vol. 9, 42 325–42 332, 2021.

[5] Chen, D., Y. Liu, S.-L. Chen, P.-Y. Qin, and Y. J. Guo, "A wideband high-gain multilinear polarization reconfigurable antenna," *IEEE Transactions on Antennas and Propagation*, Vol. 69, No. 7, 4136–4141, Jul. 2021.

[6] Nikolaou, S., R. Bairavasubramanian, C. Lugo, I. Carrasquillo, D. C. Thompson, G. E. Ponchak, J. Papapolymerou, and M. M. Tentzeris, "Pattern and frequency reconfigurable annular slot antenna using PIN diodes," *IEEE Transactions on Antennas and Propagation*, Vol. 54, No. 2, 439–448, Feb. 2006.

[7] Zohur, A., H. Mopidevi, D. Rodrigo, M. Unlu, L. Jofre, and B. A. Cetiner, "RF MEMS reconfigurable two-band antenna," *IEEE Antennas and Wireless Propagation Letters*, Vol. 12, 72–75, 2013.

[8] Yu, Y., J. Xiong, H. Li, and S. He, "An electrically small frequency reconfigurable antenna with a wide tuning range," *IEEE Antennas and Wireless Propagation Letters*, Vol. 10, 103–106, 2011.

[9] Shirazi, M., J. Huang, T. Li, and X. Gong, "A switchable-frequency slot-ring antenna element for designing a reconfigurable array," *IEEE Antennas and Wireless Propagation Letters*, Vol. 17, No. 2, 229–233, Feb. 2018.

[10] Chen, Z., B. Shao, J. Xu, G. Xu, and Y. Chen, "A high-gain tri-band patch antenna with two independent frequency-reconfigurable bands," *IEEE Antennas and Wireless Propagation Letters*, Vol. 23, No. 11, 3589–3593, Nov. 2024.

[11] Li, T., H. Zhai, X. Wang, L. Li, and C. Liang, "Frequency-reconfigurable bow-tie antenna for Bluetooth, WiMAX, and WLAN applications," *IEEE Antennas and Wireless Propagation Letters*, Vol. 14, 171–174, 2015.

[12] Chen, S.-L., F. Wei, P.-Y. Qin, Y. J. Guo, and X. Chen, "A multilinear polarization reconfigurable unidirectional patch antenna," *IEEE Transactions on Antennas and Propagation*, Vol. 65, No. 8, 4299–4304, Aug. 2017.

[13] Wong, H., W. Lin, L. Huitema, and E. Arnaud, "Multi-polarization reconfigurable antenna for wireless biomedical system," *IEEE Transactions on Biomedical Circuits and Systems*, Vol. 11, No. 3, 652–660, Jun. 2017.

[14] Tran, H. H., N. Nguyen-Trong, T. T. Le, A. M. Abbosh, and H. C. Park, "Low-profile wideband high-gain reconfigurable antenna with quad-polarization diversity," *IEEE Transactions on Antennas and Propagation*, Vol. 66, No. 7, 3741–3746, Jul. 2018.

[15] Tran, H. H., N. Nguyen-Trong, T. T. Le, and H. C. Park, "Wideband and multipolarization reconfigurable crossed bowtie dipole antenna," *IEEE Transactions on Antennas and Propagation*, Vol. 65, No. 12, 6968–6975, Dec. 2017.

[16] Chen, X. and Y. Zhao, "Dual-band polarization and frequency reconfigurable antenna using double layer metasurface," *AEU — International Journal of Electronics and Communications*, Vol. 95, 82–87, 2018.

[17] Nguyen-Trong, N., A. Piotrowski, L. Hall, and C. Fumeaux, "A frequency- and polarization-reconfigurable circular cavity antenna," *IEEE Antennas and Wireless Propagation Letters*, Vol. 16, 999–1002, 2017.

[18] Scarborough, C. P., D. H. Werner, and D. E. Wolfe, "Compact low-profile tunable metasurface-enabled antenna with near-arbitrary polarization," *IEEE Transactions on Antennas and Propagation*, Vol. 64, No. 7, 2775–2783, Jul. 2016.

[19] Ma, R., X. Li, H. Huang, and X. Wang, "A high-performance antenna with simultaneous frequency and polarization reconfigurability," *IEEE Antennas and Wireless Propagation Letters*, Vol. 23, No. 12, 4203–4207, Dec. 2024.

[20] Han, S., Z. Wang, and Y. Dong, "Miniaturized circularly polarized reconfigurable capacitance-loaded patch antenna," *IEEE Antennas and Wireless Propagation Letters*, Vol. 23, No. 4, 1226–1230, Apr. 2024.

[21] Liu, M., S. Chen, Z. Zhao, H. Chu, P. Xiao, and G. Li, "A polarization-and frequency-reconfigurable transparent liquid antenna," *IEEE Antennas and Wireless Propagation Letters*, Vol. 23, No. 8, 2281–2285, Aug. 2024.

[22] Feresidis, A. P., G. Goussetis, S. Wang, and J. C. Vardaxoglou, "Artificial magnetic conductor surfaces and their application to low-profile high-gain planar antennas," *IEEE Transactions on Antennas and Propagation*, Vol. 53, No. 1, 209–215, Jan. 2005.

[23] Feng, D., H. Zhai, L. Xi, S. Yang, K. Zhang, and D. Yang, "A broadband low-profile circular-polarized antenna on an AMC reflector," *IEEE Antennas and Wireless Propagation Letters*, Vol. 16, 2840–2843, 2017.

[24] AboEl-Hassan, M., A. E. Farahat, and K. F. A. Hussein, "Wideband star-shaped antenna based on artificial magnetic conductor surface for unidirectional radiation," *AEU — International Journal of Electronics and Communications*, Vol. 189, 155603, 2025.

[25] Malekpoor, H. and M. Hamidkhani, "Performance enhancement of low-profile wideband multi-element MIMO arrays backed by AMC surface for vehicular wireless communications," *IEEE Access*, Vol. 9, 166 206–166 222, 2021.

[26] Dai, Z. F., Y. Pan, J. J. Huang, L. H. Ye, J.-F. Li, and H. Jiang, "Low-profile broadband dual-polarized dipole antenna with AMC reflector," *IEEE Antennas and Wireless Propagation Letters*, Vol. 23, No. 11, 3496–3500, Nov. 2024.

[27] Liu, Q., H. Liu, W. He, and S. He, "A low-profile dual-band dual-polarized antenna with an AMC reflector for 5G communications," *IEEE Access*, Vol. 8, 24 072–24 080, 2020.

[28] Gong, Y., S. Yang, B. Li, Y. Chen, F. Tong, and C. Yu, "Multiband and high gain antenna using AMC ground characterized with four zero-phases of reflection coefficient," *IEEE Access*, Vol. 8, 171 457–171 468, 2020.